RESEARCH ARTICLE

John E. Bailey · Andrew J. L. Harris ·
Jonathan Dehn · Sonia Calvari · Scott K. Rowland

The changing morphology of an open lava channel on Mt. Etna

Abstract An open channel lava flow on Mt. Etna (Sicily) was observed during May 30–31, 2001. Data collected using a forward looking infrared (FLIR) thermal camera and a Minolta-Land Cyclops 300 thermal infrared thermometer showed that the bulk volume flux of lava flowing in the channel varied greatly over time. Cyclic changes in the channel's volumetric flow rate occurred over several hours, with cycle durations of 113–190 min, and discharges peaking at $0.7 \ m^3 \ s^{-1}$ and waning to $0.1 \ m^3 \ s^{-1}$. Each cycle was characterized by a relatively short, high-volume flux phase during which a pulse of lava, with a well-defined flow front, would propagate down-channel, followed by a period of waning flow during which volume flux lowered. Pulses involved lava moving at relatively high velocities (up to $0.29 \ m \ s^{-1}$) and were related to some change in the flow conditions occurring up-channel, possibly at the vent. They implied either a change in the dense rock effusion rate at the source vent and/or cyclic-variation in the vesicle content of the lava changing its bulk volume flux. Pulses would generally overspill the channel to emplace pāhoehoe overflows.

J. E. Bailey (✉) · A. J. Harris · S. K. Rowland
Hawai'i Institute of Geophysics and Planetology,
University of Hawai'i at Manoa,
Honolulu, HI 96822, USA
e-mail: jbailey@gi.alaska.edu
Tel.: +1-808-474-6504
Fax: +1-808-474-6332

J. Dehn
Alaska Volcano Observatory/University of Alaska,
Fairbanks, AK 99775, USA

S. Calvari
Instituto Nazionale di Geofisica e Vulcanologia – Sezione di Catania,
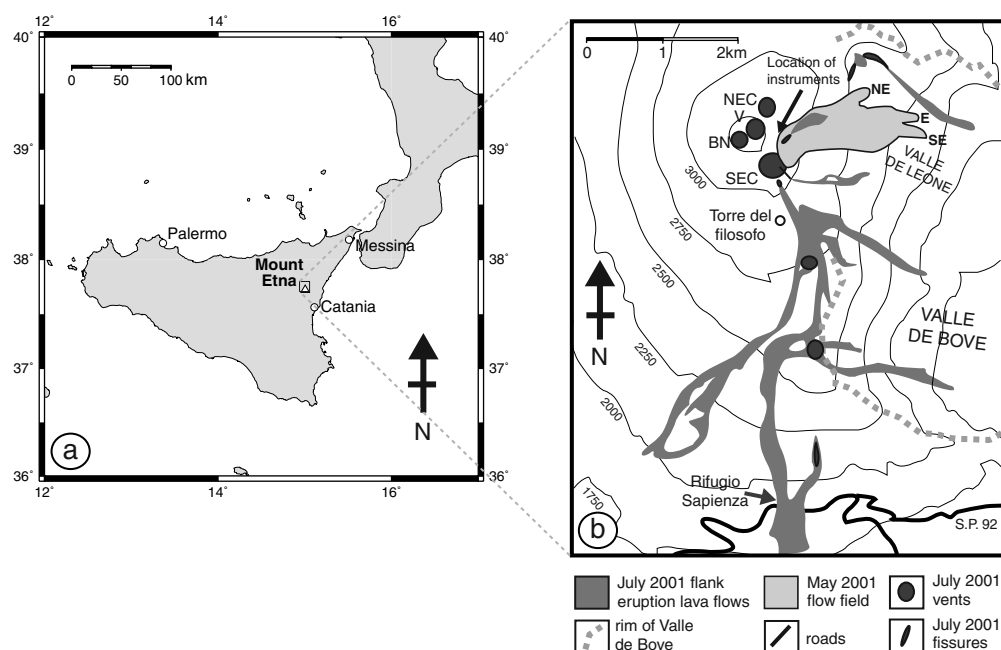Piazza Roma 2,
95123 Catania, Italy

Present address:
J. E. Bailey
Alaska Volcano Observatory/University of Alaska,
Fairbanks, AK 99775, USA

During periods of waning flow, velocities fell to $0.05 \ m \ s^{-1}$. Blockages forming during such phases caused lava to back up. Occasionally backup resulted in overflows of slow moving 'a'ā that would advance a few tens of meters down the levee flank. Compound levees were thus a symptom of unsteady flow, where overflow levees were emplaced as relatively fast moving pāhoehoe sheets during pulses, and as slow-moving 'a'ā units during backup. Small, localized fluctuations in channel volume flux also occurred on timescales of minutes. Volumes of lava backed up behind blockages that formed at constrictions in the channel. Blockage collapse and/or enhanced flow under/around the blockage would then feed short-lived, wave-like, down-channel surges. Real fluctuations in channel volume flux, due to pulses and surges, can lead to significant errors in effusion rate calculations.

Keywords Etna · FLIR · Lava channel · 'a'ā · Thermal · Unsteady flow · Morphology

Introduction

The flow regime within channelized basaltic lava flows is known to change over timescales of days, minutes and hours (Wadge 1981; Lipman and Banks 1987; Rossi 1997; Harris et al. 2000; Lautze et al. 2004). Some studies have been able to track short-term changes in lava channel morphology, volume flux, cooling rates or crystallization (e.g., Lipman and Banks 1987; Crisp and Baloga 1994; Crisp et al. 1994; Cashman et al. 1999). However, interpretation and modeling of channels on timescales of <1 day has been limited by a lack of field-based measurements of sufficient temporal or spatial coverage to show critical changes (Baloga and Pieri 1986). In this regard, field measurements are limited by the observers' ability to continually record and accurately describe changes at ephemeral, rapidly evolving, complex, or short-lived features. Ideally, such studies would collect continuous, simultaneous measurements of temperatures

498

Fig. 1 **a** Mount Etna location map. **b** Lava flow fields erupted at Mount Etna during 2001 (modified from Behncke and Neri 2003). SEC = Southeast crater; BN = Bocca Nuova; V = Voragine; NEC = Northeast Crater

and lava samples along an extended length of channel. With the notable exception of Cashman et al. (1999), such an analysis requires multiple instruments, many (or fast moving) personnel and perfect/ideal conditions.

Such measurements are, however, essential if we are to adequately understand, interpret, and model lava flow emplacement. Many studies of channelized flows at Mt. Etna (Sicily, Italy) and other effusive basaltic volcanoes, primarily Kilauea and Mauna Loa (Hawaii) have been directed towards defining parameters for quantitative modeling of flows. Hulme (1974), Dragoni et al. (1986, 1992), Dragoni (1989), Dragoni and Tallarico (1994), Pinkerton and Wilson (1994), Keszthelyi (1995) and Tallarico and Dragoni (1999), for example, studied aspects of flow emplacement and cooling to consider the impact of channel dimensions, lava cooling, crystallization, and other rheological properties on flow length, velocity and volumetric rate. In addition, analysis and modeling of heat loss from channelized and 'a'ā flows has been completed by Dragoni (1989), Crisp and Baloga (1990), Ishihara et al. (1990), Crisp and Baloga (1994), Harris et al. (1998), Keszthelyi and Self (1998), Cashman et al. (1999), and Harris and Rowland (2001).

The last 3 years has seen an increasing use of the hand-held forward-looking infrared (FLIR) thermal camera (Dehn et al. 2001). The FLIR's versatility has led to its use in many areas of thermal volcanological research, such as the analysis of active eruption plumes (McGimsey et al. 1999; Dehn et al. 2002), explosive and effusive eruptions (Dehn et al. 2003; Andronico et al. 2004; Harris et al. 2005), lava lakes (Oppenheimer and Yirgu 2002), and instability of volcanoes (Bonaccorso et al. 2003). This device is capable of collecting images of large flow-field areas. Each image is comprised of 320×240 pixels, each providing a calibrated temperature value between
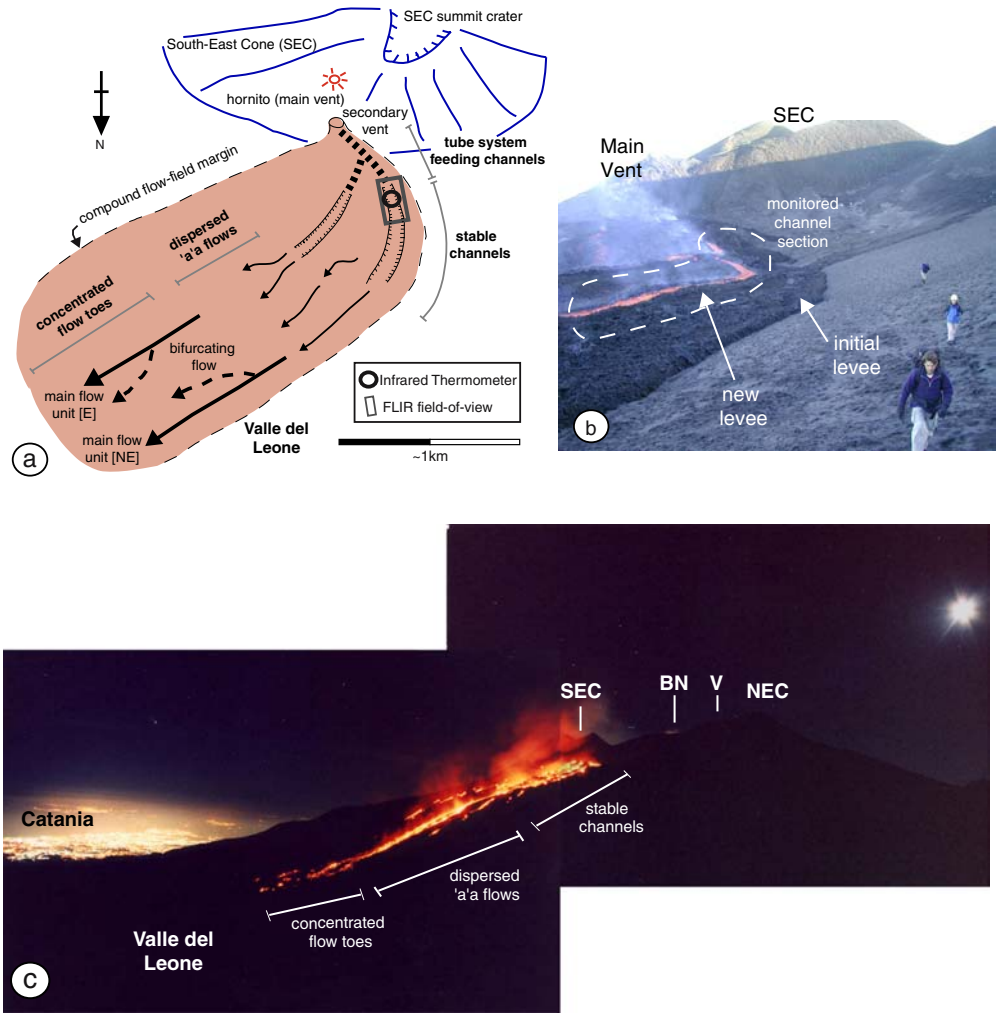
200 and 1,000°C. FLIR data thus provide a means to both qualitatively and quantitatively study the thermal history of an evolving or cooling lava flow (Keszthelyi et al. 2003; Patrick et al. 2003; Wright and Flynn 2003).

In this study, we use FLIR data, visual observations, and thermal infrared thermometer data to describe the temporal evolution of a channelized lava flow during the May 2001 eruption of Mt. Etna (Fig. 1). We begin by reviewing previous studies of Etnean flow fields and channelized basaltic flows before giving a description of the events surrounding the formation of the lava channel on which we focus. This is followed by a description of the observed channel as well as measurements made and the terminology used to describe the channel's morphology. Finally, we detail qualitative and quantitative changes in the channel morphology that result from random and cyclic fluctuations in the bulk volume flux. Our ultimate goal was thus to describe pulses observed in the volume flux, and to define what these variations imply about the system, as well as to consider the effect that volume flux changes on the order of minutes to hours have on flow rate calculations. These observations directly contradict any assumption of a steady-state flow used for modeling channelized basaltic lava flows or in making ground-based flow rate calculations. In completing our examination of a channel's morphological evolution, we also highlight the ability of the FLIR camera to provide both numerical and visual image data capable of documenting rapid morphological and flow regime changes.

The May 2001 lava flow field

Our measurements took place during May 30–31, 2001, along a length of channel in the proximal section of a flow field being emplaced on the NE flank of the South-East

Fig. 2 **a** Schematic overview of the NE branch of the May 2001 flow field showing the flow zones and measurement areas for this study. **b** Photograph of NE margin of flow field and monitored channel section. **c** Night time photograph of the flow field on May 30 showing the main flow zones. View is looking to the SW over a distance of ~2 km

Crater (SEC), within the upper Valle del Leone between 3,000 and 2,500 m elevation (Figs. 1 and 2). At this time, the flow field as a whole was being fed at an effusion rate of 1.4 ± 0.4 m³ s⁻¹ to build a 2.5×1 km (~2.5 km²) flow field. We use the term 'effusion rate,' as defined in Calvari et al. (2002), to describe the estimated instantaneous total rate at which lava is erupted for the whole flow field. This effusion rate may be divided between a number of channels. The term 'flow rate' refers to the rate of lava discharge through a given channel. Thus, where multiple channels exist, the channel flow rate will be less than the at-vent effusion rate. Figure 3 shows effusion rates recorded for May and June 2001. The data are derived from satellite (AVHRR) and ground-based measurements by Lautze et al. (2004).

By May 30, the lava flow field comprised four main sections. The first section was a zone of stable tube that extended ~0.5 km from a series of vents on the NE flank of the SEC. This tube bifurcated 0.25 km from the vent to feed two channels (Fig. 2). These comprised the second flow field section: a zone of stable channelized flow. This in turn fed the third section, a zone of dispersed 'a'ā flow, which fed the fourth section, three main lobes at the distal portion of the flow field.
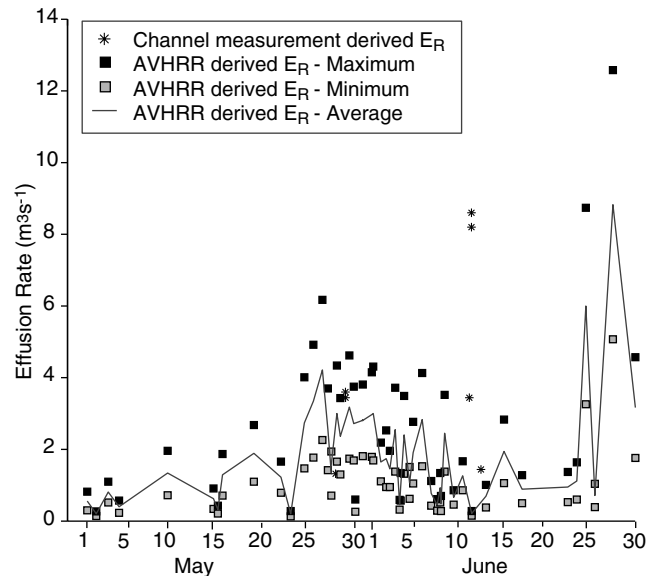

Fig. 3 Effusion rates during May and June (2001) derived from satellite (AVHRR) and ground-based measurements by Lautze et al. (2004)

Activity at the SEC had been continuous but at variable levels since January 2001 (Lautze et al. 2004). Emplacement of the channel-fed flow field, however, occurred mostly during May 2001, and correlated with a period of increasing effusion rates (Fig. 3). During the first week of May, weak spattering produced hornitos along a fissure located on the NNE flank of the SEC (Behncke and Neri 2003). These were initially the sources of low-volume effusive activity. Strombolian activity at the summit of the SEC began late on the morning of May 7, and at 16:30 (all times are local) on May 9 the SEC's first fire-fountaining event of 2001 began. The cessation of fountaining was followed by additional effusive activity, where flows erupted from the NNE flank fissure rapidly extended towards the east.

For the next week (May 10–17) persistent effusive output continued from the NNE fissure, sometimes from more than one spattering vent. By May 15, the active flow extended over 1 km into the Valle del Leone (Fig. 1). At about 19:00 on May 17 the intensity of activity increased, and by May 18 lava effusion had become focused at a single vent, a hornito at 3,156 m elevation on the flank of the SEC. Lava flow continued at an effusion rate of 2–3 $m^3 s^{-1}$ (Fig. 3) to feed a flow that split into three branches a short distance below the hornito. One of these branches extended to the NE with a flow front that reached a distance of about 1 km from the vent. This NE branch remained active through our observation period and was the focus of our study. The central branch flowed to the east, and was the widest of the three. The third branch flowed to the ESE, traveling about 700 m from the vent.

Continuous flow persisted over the next 10 days. However, activity at the NE branch diminished greatly in intensity. Along the upper part of this flow, sluggish lobes were issued out of a tumulus that developed 150 m down-slope from the main effusive vent, but these lobes did not advance farther than ∼500 m down-slope. The ESE branch crusted over to form a tube over part of its length. Activity in the east flow in contrast remained strong, fed by a constant source of lava from the 3,156 m hornito. During this period, changes in effusion rate were noticed with new material occasionally rapidly over-running older slower-moving flow fronts.

By May 28–30 the effusion rate increased to 2–6 $m^3 s^{-1}$ (Fig. 3). Activity was particularly strong at the NE and E branches, where channel-fed 'a'ā flows extended >2.0 km into the Valle del Leone (Fig. 1). Through June 6 flows continued to extend 2.3–2.5 km into the Valle del Leone, by far the longest branches that had thus far been recorded during activity in 2001. The increased effusion rate was also mirrored by an increase in Strombolian events within the SEC. This increase culminated in a series of 14 fire-fountaining episodes that occurred between June 7 and July 13. These fire-fountaining episodes were merely a forerunner to a large flank eruption, which began on July 17 and emplaced a 4.7 km^2 flow field primarily on Etna's south flank (Fig. 1; Calvari et al. 2001; Behncke and Neri 2003).
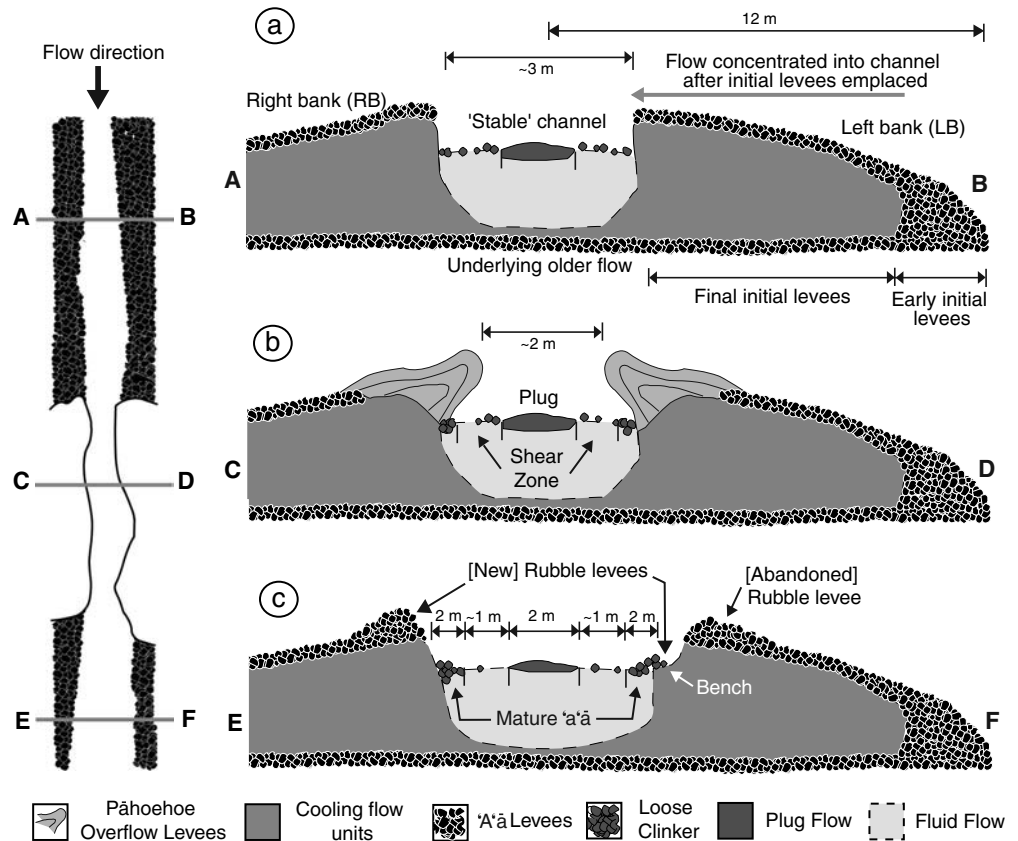
Channelized 'a'ā flows on Etna

Macdonald's (1953) description of 'a'ā lava can be paraphrased as "lava with a rough, jagged, spinose and generally clinkery surface". Based on this description, virtually all of Etna's historical flows can be classified as 'a'ā (Kilburn 1990). Exhaustive descriptions of the lava types and textures found on Etna are given in Kilburn (1990, 2000) and by Kilburn and Guest (1993). Commonly Etna's lava flows form compound flow fields (Walker 1972), comprised of multiple 'a'ā flow units. On the steeper slopes, flow is generally maintained through channels or tubes (Calvari and Pinkerton 1998), whereas shallower slopes encourage dispersed, bifurcating and braiding flows, due to a decrease in mean flow velocity and subsequent adjustment to new rheological conditions and flow front inflation (Polacci and Papale 1997; Calvari and Pinkerton 1998).

The high frequency of eruptions on Mt. Etna has allowed numerous studies of flow-field formation. Some of these studies have concentrated on overall flow-field morphology or its formation chronology, using either field-based measurements, e.g., Pinkerton and Sparks (1976), Frazzetta and Romano (1984), Guest et al. (1987), Kilburn and Lopes (1988), Calvari et al. (1994), Calvari et al. (2002), Behncke and Neri (2003), or remote sensing data, e.g., Pieri et al. (1990), Harris et al. (1997, 2000), Wright et al. (2000, 2001). Other studies have concentrated on changes within the channelized or tubed sections of a flow. Calvari and Pinkerton (1998, 1999), for example, described the morphology and mechanism of formation of lava tubes on Etna, Polacci and Papale (1997) performed post-emplacement studies of flow units fed by lava tube emission points, and Kilburn and Guest (1993) described textural variations for Etnean 'a'ā and pāhoehoe flows.

A small group of studies have focused on the morphology of channel levees, setting out a series of definitions that are important to our study. Static marginal levees between which a central zone of lava continues to move are common features of 'a'ā flows (Hulme 1974). Sparks et al. (1976) described four different types of Etnean levee: initial, accretionary, rubble and overflow. Initial levees are formed by the stagnation and cooling of lava at the margins of the initial flow unit (Hulme 1974; Sparks et al. 1976), and are characterized by a broad zone of marginal clinker bounding the central flowing plug (Figs. 2 and 4). Effectively these are the rubbly flanks of the 'a'ā flow left behind after the initial flow passed through (Lipman and Banks 1987). Naranjo et al. (1992) point out that narrowing of the actively flowing central zone results in inward growth of the initial levees, an effect we observe in the morphologies of our channel levees (Fig. 4). Formation of 'a'ā clinker at the flow margins by shearing and milling results in piles of clinker being gradually piled up at the margins of the flow zone (Naranjo et al. 1992). This process is responsible for rubble levees (Sparks et al. 1976) that overlie the inner edge of the initial levee. Continued narrowing of the central flow zone can leave a series of abandoned rubble levees that attest to sustained inward levee growth, as observed at the

Fig. 4 Typical flow profiles through the channelized flow zone and upper zone of the transitional channel
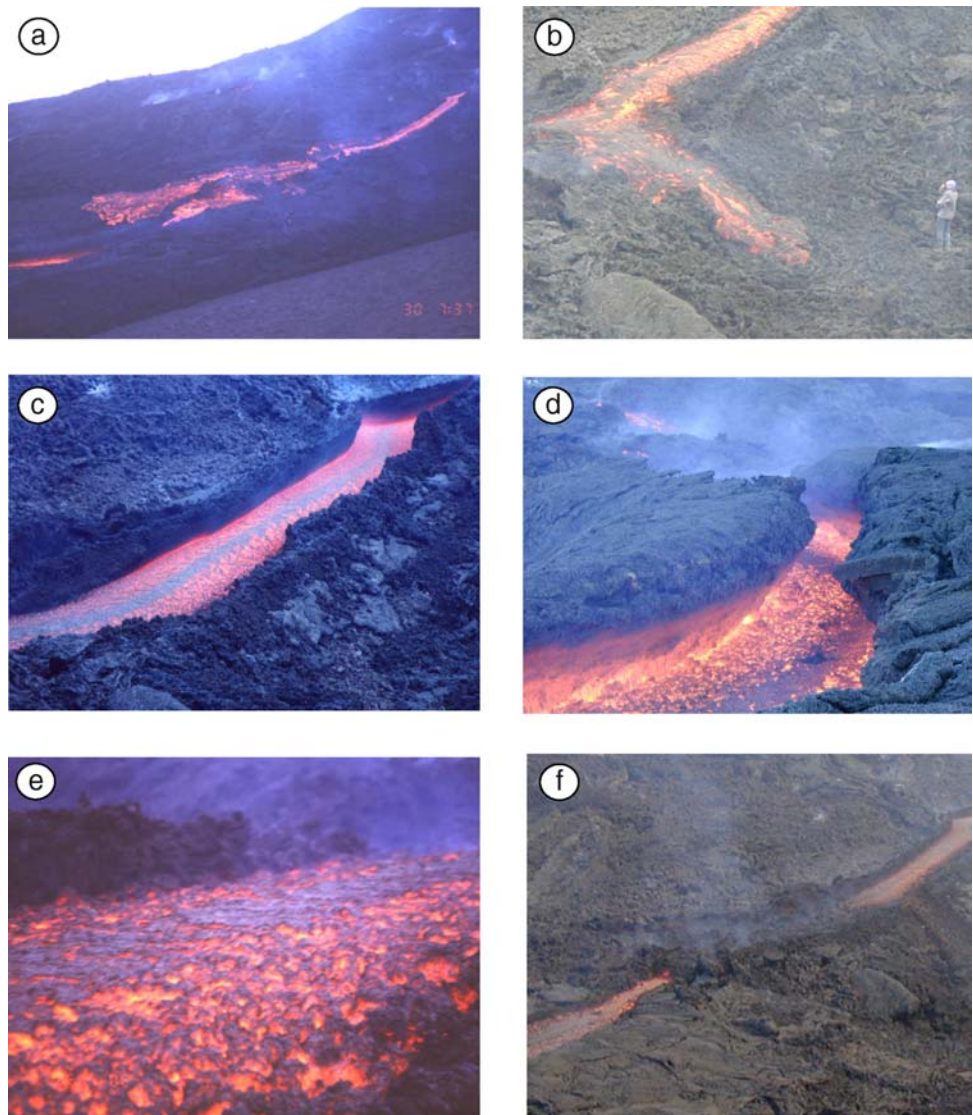

2001 Etna channel (Fig. 4). However, pulses of increased bulk lava supply moving down the channel or blockages can cause short term lateral overflows to build overflow levees that also cap the initial levees (Sparks et al. 1976; Lipman and Banks 1987). As we describe later, pulses produced overflows of pāhoehoe (Fig. 5a), whereas blockages produced 'a'ā overflows (Fig. 5b). During pulse-related overflows, accretion of pāhoehoe lava to the inner wall and lip of the channel also contributed to accretionary levees (Sparks et al. 1976) that result in overhanging channel walls (Fig. 4).

The Lipman and Banks (1987) study of the 1984 Mauna Loa channel also provides an important source of comparison for this study, because many of the morphologies observed at Mauna Loa were also apparent at the May 2001 Etna flow. Lipman and Banks (1987) provide a useful spatial framework within which morphologies characteristic to certain, increasingly distal and immature channel sections can be placed. Based on the concept of Lipman and Banks (1987) we identify and divide the Etna channel into four zones characterized by systematic down-channel evolution in structure and morphology. These are (from vent-to-toe): stable channel flow, transitional channel, dispersed flow, and flow toe (Fig. 2). In effect, the down-flow transition from one zone to another is a reflection of decreasing maturity. The channelized flow zone characterized the upper section of the ~2.5 km long flow. It was fed by a tube whose exit was located ~440 m from the main vent. In

this ~580-m-long section, all marginal motion had ceased, and flow was concentrated in a single channel of relatively consistent geometry. The channel was relatively narrow (~3 m wide) with 20 to 30-m-wide initial levees capped by pāhoehoe and 'a'ā overflows. These overflows typically extended laterally ~5–20 m from the channel and added to the complex, compound nature of the channel's levees. The inner-channel walls were approximately vertical (Fig. 5c). Through time, accretion produced overhanging levees (Figs. 4 and 5d). The flow surface moving within the channel was characterized by a central slab of pāhoehoe bounded by zones of 'a'ā clinker formation.

Across the transitional channel zone, lava flow still occurred in a distinct channel, but the levees seen were complex. They resembled initial and rubble levees (Sparks et al. 1976; Fig. 4c). The central channel was wider (6–10 m wide), and extended an additional ~580 m down flow. Newly formed rubble levees (Fig. 4c) attained heights of 1–1.5 m and widths of 4 m. With increasing distance down this section, the central pāhoehoe slab died out and the flow surface developed a complete cover of 'a'ā clinker. This clinker coverage evolved down-flow from marginal bands of brittle 'a'ā clinker bounding shear zones of plastic clinker (Fig. 4). Down-flow from the transitional channel zone was a zone of dispersed flow, characterized by a ~970-m-long zone of braided 'a'ā flow within which channels were absent (Fig. 2). The toe zone consisted of an extreme distal zone of constant flow crumbling to feed incandescent

Fig. 5 **a** Vigorous over bank pāhoehoe sheet flow during a down-channel pulse of lava. Length of channel section is ~200 m and the upper section of the stable channel zone. **b** Sluggish 'a'ā overflow upslope of a blockage. The overflow is ~2 m wide. **c** Near vertical-walled channel in upper stable channel zone during May 30, showing well-developed plug flow characterized by central zone of plastic pāhoehoe and embryonic 'a'ā forming in the marginal shear zones. Channel is ~3 m wide. **d** Lower reach of the channel zone on May 31 showing well developed plug flow and over-hanging accretionary levees, overhang angle is ~60°. Up-flow the channel has completely zippered-up. **e** Close up of the marginal shear zone showing plastic balls of clinker forming and rolling, with more coherent, plastic pāhoehoe crust forming at the central plug. Channel is ~3 m wide. **f** Rubbly blockage forming in the channel during a phase of sluggish flow

avalanches that extended a further few tens of meters down-slope from the actual flow front. The steep slope (up to ~20°) over which the flows were extending promoted the crumbling and avalanching.

Instrumentation and data collection

Visual observations of the channel were made throughout daylight hours over May 30 and 31. In addition, a FLIR Systems ThermaCam PM 595 and a Minolta-Land Cyclops 300 thermal infrared thermometer recorded thermal data for the channel surface during the same 2-day period. The two instruments were tripod-mounted to ensure stable targeting ~100 m from the channel (Fig. 2).
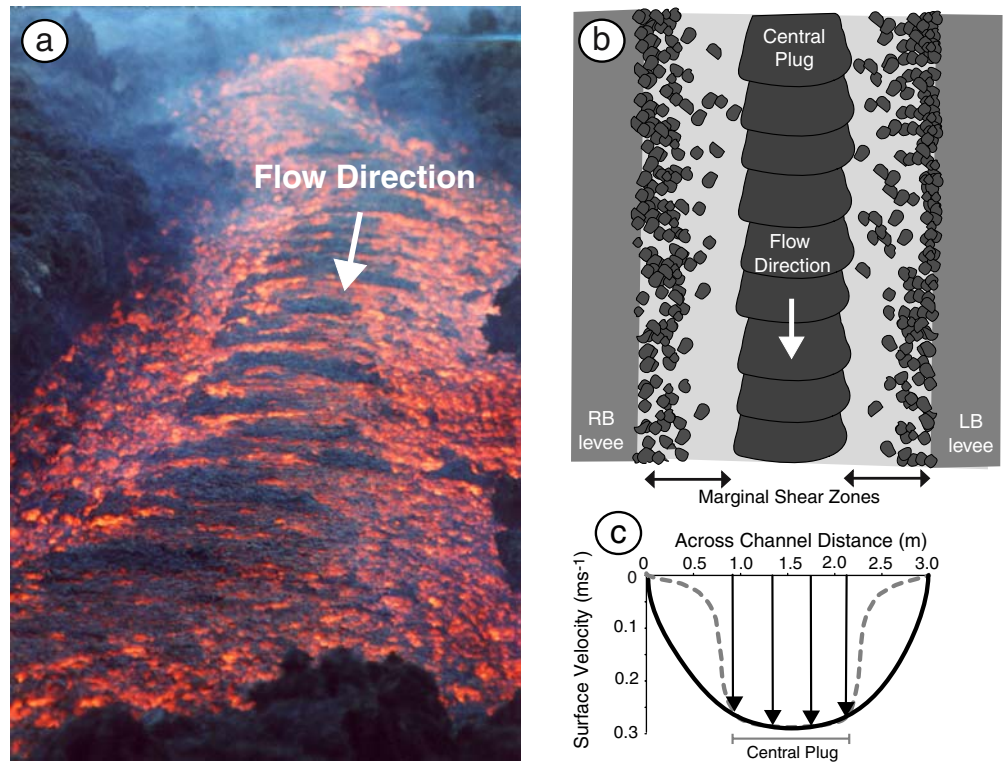
The FLIR ThermaCam 595 is operable in different modes (Dehn et al. 2003) and images can be collected as often as once every second. We used sample rates of 10, 15 and 30 s to maximize temporal coverage, which was limited by the FLIR battery's lifetime. A total of 2,106 images (324 MB of data) were collected covering 3.73 h and 4.18 h on May 30 and 31, respectively. Within the images, each pixel represents a FLIR temperature that is automatically corrected for surface and path length effects using a line-of-sight distance, humidity, air temperature, and emissivity, all of which are input at the beginning of each data collection run. At the line of sight distance in this study (~100 m), each pixel area corresponds to an instantaneous field of view (IFOV) of 0.13 m. However, this assumes that FLIR viewing was perpendicular to the target, which was not the case. It was therefore necessary to use trigonometry to perform a geometric adjustment of this value before using it to compute real distances from measurements made in pixels on the FLIR images. For cross-channel width measurements this adjustment was:

$$\text{Pixel width (m)} = \text{IFOV}/\cos\theta \qquad (1)$$

where θ is the angle of intersection between the FLIR's line-of-sight the long axis of the channel. The width was measured at the center of the FLIR image, where

Fig. 6 a Photo and **b** schematic diagram of plug flow surface features in the channel (width is ~3 m). **c** Velocity profile obtained following Cigolini et al. (1984) and Harris et al. (2002). Profile (*black line*) has been modeled for a flow width of 3 m and a maximum velocity of 0.29 ms⁻¹. An adaptation (*dashed gray line*) is suggested to show that in the field we observed (almost) static zones at the channel margins due to the growth of fixed crust, This a type of "roof" growth, which can lead to tube formation (Peterson et al. 1994)

$\theta = 72°$. For along-channel measurements the geometric adjustment was:

$$\text{Pixel length(m)} = \text{IFOV}/\sin\theta \qquad (2)$$

However, these adjustments were complex, as the FLIR has a field of view (FOV) of 24° (12° either side of the line of sight), which meant across the image θ varied from 84° at the near (down-flow) edge to 60° at the far (up-flow) edge. The more acute θ becomes, the larger the pixel length ($=\infty$ at $\theta = 0°$).

Thermal infrared thermometer data were collected once every 5 s on May 30 for a period of 6 h, and once every 2 s on May 31 for a period of 6.5 h. The thermal infrared thermometer provides an integrated value of radiance for a flow surface area defined by a 1° FOV. Over a distance of 100 m this corresponds to a circular area of 2.43 m². This spot was centered in the lava channel and, given a channel width of ~3 m, meant that the flowing section of the channel completely filled the FOV. The output data were un-corrected brightness temperatures.

Methodology

The FLIR image data were used in two ways. The first was to extract channel dimensions, flow velocity, effusion rate and plug width. The second was to track and describe changes in channel morphology over time, in combination with visual observations.

The central plug was identified as a zone of cooler pixels in the central part of the channel (Fig. 6). The plug width (w_p) was measured as a number of pixels and then multiplied by the calibrated pixel dimension to obtain width in meters. Surface flow velocity was similarly calculated from the distance a piece of identifiable crust traveled in a known time. This velocity was usually that of the flow centerline, and therefore a maximum flow velocity (v_{max}). If we approximate the channel as a half cylindrical conduit of radius d (Walker 1967; Dragoni et al. 1986; Calvari et al. 1994), and a parabolic flow profile is assumed (Tallarico and Dragoni 1999; Kerr 2001), an estimate of bulk volume flux (B_{flux}) can be made following Calvari et al. (2002):

$$B_{flux} = 0.67(v_{max}A) \qquad (3)$$

$$A = 0.5(\pi d)^2 \qquad (4)$$

where d = depth of the flow at mid-channel, measured by pushing a length of re-bar into the lava until the channel floor was found. Since the value of d changes, this method only provides a spot measurement approximation of B_{flux} for different times of flow. Errors are similar to those in Calvari et al. (2002), cumulatively ±40%.

Observations of the stable channel flow zone

Our 2001 Etna observations were made within the upper channel zone, where we focused on examining the evolution of this apparently stable channel flow section. This section was thus within the proximal section of the overall flow field and was linked to the main vent by a short section of tube (Fig. 2). Although 'stable' within the definition of Lipman and Banks (1987) the channel showed significant morphological and flow regime fluctuation during our 2-day observation period.

As we show, the activity along what in post-eruption analysis would be considered stable channel flow shows considerable temporal variability. Accumulation of solidified crust at channel constrictions formed blockages that were unstable and ephemeral, forming and decaying on time scales of tens of minutes. Blockages were then an initial stage of tube formation, as described in Calvari and Pinkerton (1998). These blockages were also not true blockages as they only stopped flow at the surface: flow continued beneath them. However, the blockages were large enough to impede flow such that the channel's fill level (surface of flowing lava relative to levees) was lowered downstream and a volume of lava became ponded or backed up behind the blockage.

Lipman and Banks (1987) recognized the effects that blockages had on the character of the 1984 Mauna Loa channel. They describe how the backed up lava was eventually released either by overflowing or breaking through the channel levees, or by overwhelming and flushing away the blockages. When a blockage broke down, a surge of lava propagated down the channel. Lipman and Banks (1987) called these 'lava surges' and they occurred when the weight of the backed up lava exceeded the strength of the obstruction.

At Etna we observed similar events but at two different volume scales. Small increases in the volume flux of lava due to localized release of lava backed up behind blockages were seen and are referred to as *surges*. It is important to differentiate them from larger *pulse* events. These were significant changes in the channel's bulk volume flux that appeared to be sourced by the vent and advanced along the entire reach of visible channel.

Plug flow and channel thermal structure

The flow in the channel displayed a well-formed central plug bounded by marginal shear zones (Fig. 6). The plug was typically 0.75–1.2 m wide, and was bounded by 0.9 to 1.1-m-wide shear zones. Flow had a velocity gradient from around zero at the channel edges to a maximum at the central plug (Fig. 6). Constant surface flow velocities across the plug resulted in shear forces less than skin strength, so that a coherent crust could form. The plug was usually a series of thin plates of spiny pāhoehoe (Figs. 5 and 6). The velocity gradient on either side of the plug caused shearing and as a result the crust was torn and rolled (Moore 1987; Rowland and Walker 1990; Kilburn and Guest 1993). Consequently,

the surface of the marginal shear zones was characterized by spinose, rotating, balls of pasty crust that are, in effect, incipient 'a'ā clinker (Fig. 5e) or 'a'ā cauliflower (Kilburn and Guest 1993).

This plug-dominated surface morphology resulted in a thermal structure similar to the one observed and measured by Flynn and Mouginis-Mark (1994) on Kilauea. The shear zones at Etna displayed the two component thermal structure of Crisp and Baloga (1990) with relatively cool crust separated by high temperature incandescent zones (Fig. 5 and Table 1). Material exposed at the high temperature zones was typically cooler than the flow core temperature. The maximum incandescent surface temperature was 1,042°C compared to a thermocouple-derived flow core temperature of 1,065°C (Table 1). The plug also showed a two-component thermal structure, but the crust percentage was higher, and both the crust and incandescent temperatures were cooler (Fig. 5 and Table 1).

Variations in flow velocity, plug width and surface morphology

The temperature recorded by the Minolta-Land Cyclops 300 infrared thermometer is an integrated temperature (T_{int}) described by:

$$L(\lambda, T_{int}) = pL(\lambda, T_{crust}) + (1 - p)L(\lambda, T_{high}) \qquad (5)$$

in which L is the Planck function for a blackbody radiating at wavelength λ and temperature T, p is the FOV portion occupied by cool crust at temperature T_{crust}, and T_{high} is the temperature of hot material occupying the remainder of the FOV. Thus a decrease in T_{int} (5) implied an increase in crust coverage, and/or a decrease in T_{crust} and/or a decrease in T_{high}. This is consistent with a scenario where reduced velocities are associated with wider more coherent plugs, narrower marginal shear zones, and more extensive and/or cooler crusts within the marginal shear zones. Conversely, higher velocities were associated with narrower plugs, and less extensive and/or cooler crusts, and hence higher T_{int}. Thus T_{int} can be used as a proxy for vigor (velocity) of the flow, although it is not precise as temperature change appears to lag ∼15 min behind changes in velocity. This is not unexpected for a cooling and evolving flow.

The time series of T_{int} indicated a systematic variation in flow conditions that correspond to visual observations (Fig. 7a and b). Flow in the channel showed a cyclic evolution beginning with increases in the channel level and flow velocity, which led to pulses in the bulk flux of lava. These pulses of fast moving lava, lasting a few minutes propagated down-flow with a well-defined front (Fig. 8). Peaks in the T_{int} marked such pulses as the increased flow velocity caused increased crust disruption and narrower plugs. After the pulse passed increasingly sluggish flow would develop over time scales of tens of minutes. During such periods, flow velocity would steadily decline, plug widths would increase, and T_{int} would decrease. At the same time, the channel would become increasingly

Fig. 7 **a** Thermal infrared thermometer time series shown by 50-point moving average for May 30. Coincident times when FLIR data were captured are indicated. **b** Thermal infrared thermometer time series for May 31. **c** Plug width, flow velocity and thermal infrared thermometer signals recorded during pulse-cycle 2
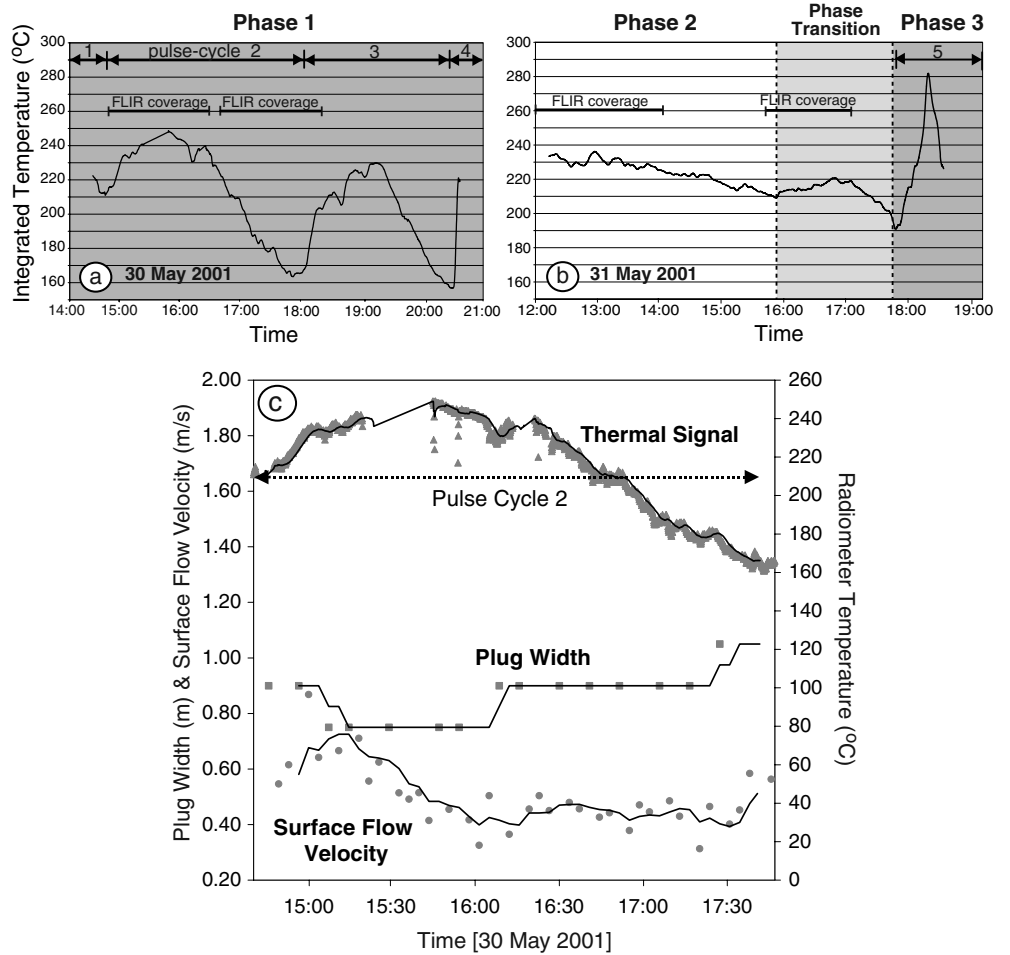

Fig. 8 Photograph of pulse propagating down the channel and overtopping the levees on May 30. Flow front is ~10 m wide
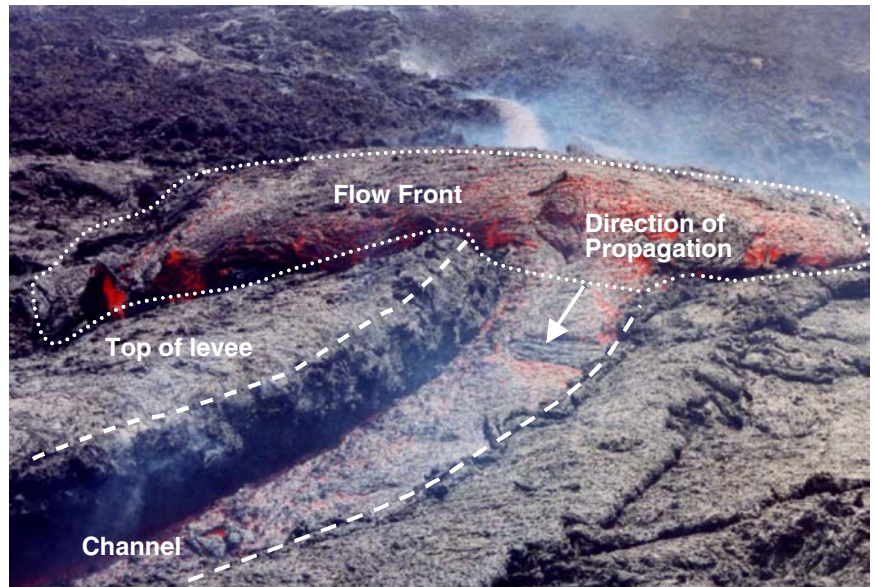
Table 1 Temperatures measured using Land/Minolta 152 thermal infrared thermometer

Core temperature was measured at 1,065°C using a k-type thermocouple

Temperature measurements	Plug zone cracks	Plug zone crust	Shear zone cracks	Shear zone crust	'A'a overflow cracks
Minimum temperature (°C)	733	658	872	676	1,008
Maximum temperature (°C)	950	831	1,042	877	1,074
Mean temperature (°C)	834	760	932	786	1,045
Standard deviation	49	34	43	43	23
Number of measurements	42	42	42	42	8

inefficient with blockages developing and the level of the surface up-flow steadily rising due to backup behind blockages. The blockages would eventually be cleared by another pulse that would mark the beginning of a new cycle.

Pulse cycles typically had a 2 to 3.5-h-long duration. Over this time scale, the surface flow velocity (v_{max}) varied from 0.05 to 0.29 m s^{-1}. Using Eq. (3) this converted to a variation in bulk volume flux (B_{flux}) of 0.1–0.7 m^3 s^{-1} (Table 2). The width of the central plug (w_p) varied from 1.2 m during periods of low flux to 0.75 m during high periods (Fig. 7c). Changes in plug width due variation in flow rate is a feature of lava channels that has been predicted by laboratory simulations (Griffiths et al. 2003).

Overflows due to flow pulses

Pulses that over-spilled the channel (Fig. 8), fed overflows spiny pāhoehoe flow units (Figs. 5a and 9). Each pulse lasted a few minutes, after which flow velocity and level declined such that flow could be accommodated within the channel once more. The pulse would propagate down the entire channel; initiating spiny pāhoehoe overflows along the way. Once the pulse moved on down-flow each overflow became starved of supply and consequently they extended no more than 20 m from the channel, and were typically <0.5 m thick.

Plastering of multiple overflows during repeated pulses caused the construction of even higher and overhanging levees (Figs. 4 and 5) such that the channel profile evolved from an approximately rectangular form to one resembling an upside-down light bulb (Fig. 4). Eventually, overhanging rims extended to completely seal the channel, forming sections of tube (Calvari and Pinkerton 1998). Pulses also flushed away blockages that had formed in the channel. The increased efficiency of the channel immediately following a pulse meant that lava was relatively free flowing and typically returned to a level below the channel rim. However, following the pulse the flow would steadily become more sluggish, leading to the formation of blockages and decreasing the lava's ability to flow freely.

Overflows due to blockages

The blockages developed at the same location during each cycle, where the channel width narrowed to 1–2 m (Fig. 9). Here solidified crust, as well as levee debris that had fallen into the channel, accumulated to form a coherent pile of rubbly material extending across the flow surface (Fig. 5f). Continued flow beneath the blockage meant that these were surficial features: roofs rather than true blockages. Sometimes these blockages continued to grow ~10 m upstream, forming a coherent roof over the channel with flow continuing beneath the roof. Usually such extended roofs were ephemeral and were destroyed during the next pulse.

By decreasing the efficiency of channel flow, blockages caused lava to backup in the channel and occasionally overflow. Such overflows were slow moving 'a'ā that moved down the outer flank of the levee (Fig. 5b). One such flow on May 31 advanced ~30 m in 15 min, giving a mean velocity of 0.03 m s^{-1}. Once a blockage collapsed or was removed by a flow pulse, the flow level dropped, and the overflows starved. Unlike the pulse-fed pāhoehoe overflows, the 'a'ā overflows due to blockages were localized, short and narrow (Fig. 9). Three of these 'a'ā overflows observed during the afternoon of May 31, for example, were 10–20 m long, 3–4 m wide and ~0.5 m high.

Flow surges

The release of lava that had backed up behind a blockage caused rapid but short-lived increases in the volume flux down-channel of the blockage. These surges propagated down-flow as small waves. Such events were often subtle, and only evident in sped up sequences of FLIR images.

They differed from pulses in that pulses appeared to emanate from the vent, whereas surges were fed by release of backed up volumes contained within the channel. In addition, the volume flux associated with surges was much lower than that with pulses; surges were always contained within the channel and did not contribute to levee construction, except for perhaps on the inner channel walls.

Table 2 Measurements calculated for actively flowing channel using measurements made on FLIR images and Eq. (1)

Channel measurement	Minimum	Maximum	Mean	Standard deviation
Maximum surface flow velocity (v_{max})	0.15 ms^{-1}	0.87 ms^{-1}	0.46 ms^{-1}	0.13 ms^{-1}
Plug width (w_p)	0.75 m	1.20 m	0.93 m	0.13 m
	Low flux flow		High flux flow	
Channel depth (h)	1.2 m		1.5 m	
Bulk volume flux (B_{flux})	0.1 m^3 s^{-1}		0.7 m^3 s^{-1}	

Fig. 9 Overview of the channelized flow section. **a** The first FLIR image collected on May 30 shows hot active flow in white and yellow, cooling overflows in orange, and cooler levees in purple and blue. The central channel and recent overflows are clearly distinguishable. Channel section is ~100 m long. **b** Schematic of the channel section, surrounding cooling overflows when observations began on May 30 and locations of subsequent blockages formation
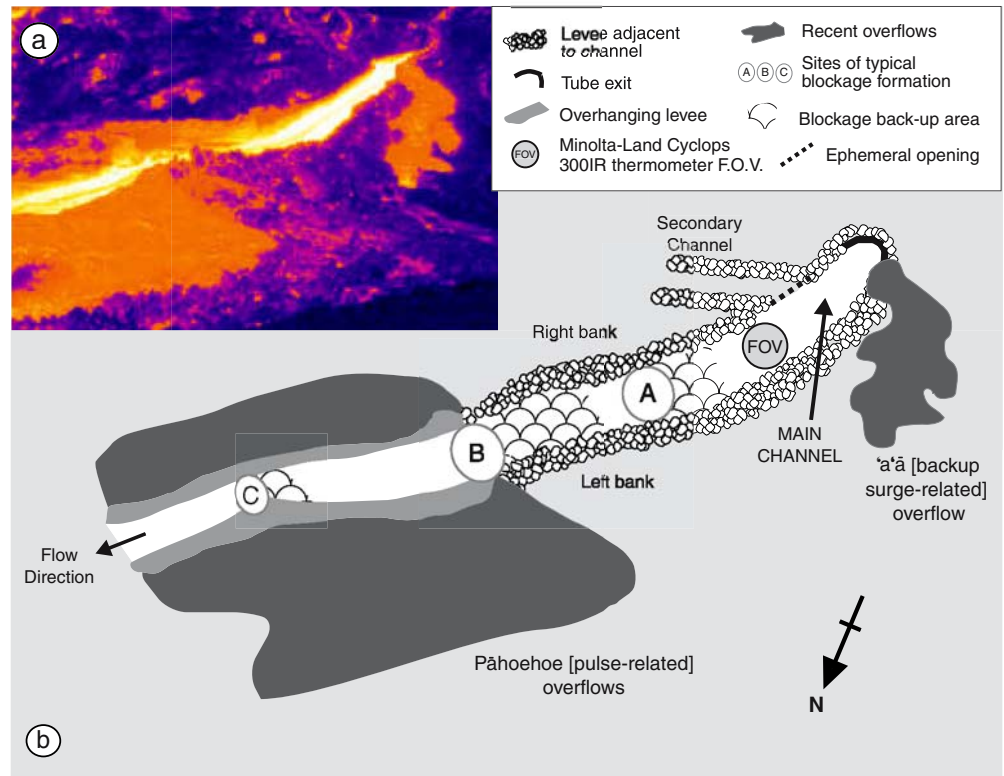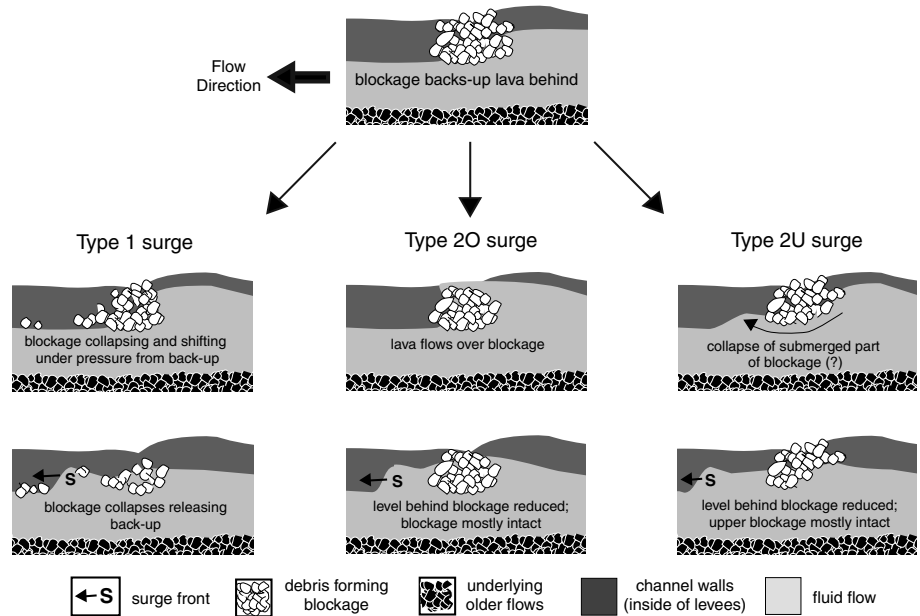

Fig. 10 Cross-sectional views showing modes of formation of type-1 (due to blockage collapse), type-2O (flow over blockage) and type-2U (flow under blockage) surges

We identified two mechanisms of surge generation. The first, a type-1 surge, involved partial or total collapse of a blockage (Fig. 10). If blockage collapse was large enough or occurred in stages multiple surges would result. Type-2 surges were generated by stronger, more substantial blockages. Again, the event involved sudden release of backed up lava that generated a down-stream wave, but in these cases the surge was generated without the blockage totally disintegrating (Fig. 10). The type-2O events resulted from lava backing-up to such an extent that is simply overtopped the blockage, whereas type-2U events may have been due to failures of submerged sections of the blockage. On some occasions, a hybrid event could occur whereby the surge started as type 2 but as the backed up lava flowed over or under the blockage it collapsed and type-1 event followed. This often created double or even triple surge-fronts.

Table 3 Pulse events observed (OF = overflow, S = surge, P = pulse, B = blockage, T = Tube)

Pulse	Date & time of observation	Events due to pulse	Cycle wavelength (min)
1	5/30/03 (∼11:30–14:40)	Pahoehoe lateral flows produced down flow of site B (OF1). A bifurcated flow (OF2) tried to form down the left bank, next to the tube exit. Temperatures measured by the FLIR indicate these occurred within 2–3 h before the start of observations	∼190
2	5/30/03 (14:40–17:49)	Channel flowed very full with a convex shape that elevated the central part of the flowing surface above the level of the levee tops. It was contained within the levees, but after the peak had passed a blockage built at B and the levee eventually failed producing a lateral flow (OF3) down the left bank, up-flow of site B	189
3	5/30/03 (17:49–20:23)	An increased volume of lava with a well-defined flow front propagated down-flow producing overspills down the right bank, and destroyed a forming lava tube (T1)	154
4	5/30/03 (20:23–n/a)	Pulse produced overflows. Cycle continued beyond instrument observation time	n/a
	5/31/03 (11:09–15:51)	No pulse occurring	n/a
	5/31/03 (15:51–17:52)	Flow level increased producing some small overspills (OF5) onto tops of levees. Solid blockage (B8) held and back-up broke through the left bank levee as a lateral flow (OF6) up-flow of site C	n/a
5	5/31/03 (17:53–19:45)	Large pulse similar to pulse 3. Destroyed blockage (B8) which had built up into a lava tube (T2) and overflowed down left bank (OF7)	113

Average cycle wavelength ∼160 min. See Figs. 11 and 12 for locations of overflows, tubes and blockages referred to here

Temporal variation in channel flow rates and morphology

Graphical representation of thermal measurements made from ∼14:30 to 20:30 on May 30 reveal an approximately sinusoidal variation related to cycles of a pulse followed waning flow (Fig. 7a and b). Each thermal cycle begins with increase to a peak related to high-integrated surface temperatures during vigorous, high velocity flow, followed by a steady decay due to a slow reduction in flow rate. All peaks corresponded to observed pulses propagating down-flow. FLIR images acquired on May 30 indicated older inactive, but recently emplaced pāhoehoe overflows. Based on the degree to which they had cooled the pāhoehoe overflows indicated that the pulsing activity had been occurring for at least several hours previous to the start of our observations. Activity was continuing in a similar style when measurements were stopped for the night.
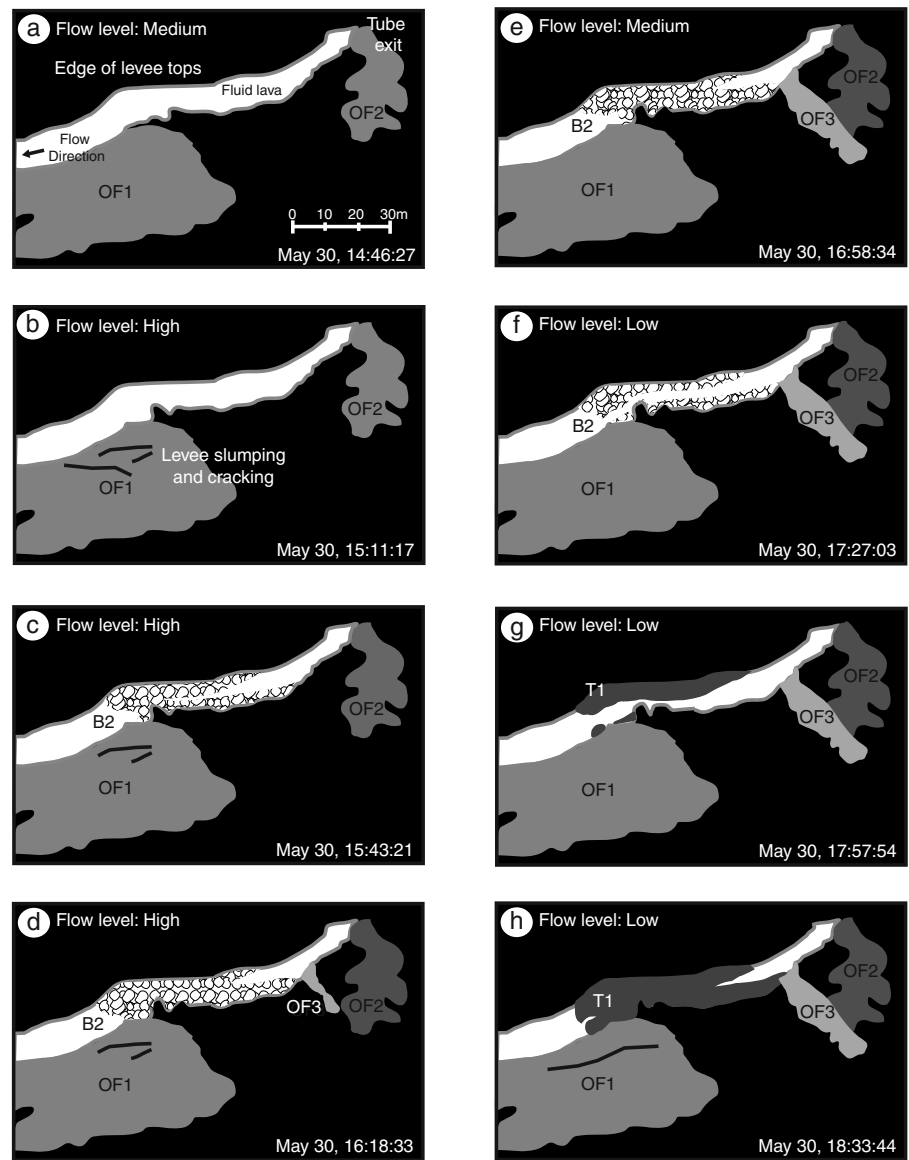
During the first 3 h of observations during May 31, flow continued at a relatively stable volume flux. Thus backup and surge-related processes associated with blockages dominated activity at the channel, because the channel was not periodically cleared of debris in the way it had been by pulses throughout May 30. A gradual decrease in the thermal output during this time related to steady stagnation of flow behind an increasingly large blockage that was able to mature during this prolonged period of non-pulsing flow (Fig. 7b). However, at 17:53 there was an upturn in the thermal trend, correlating with visual observations of a return to the periodic pattern of pulses.

This channel was thus fed at a variable rate, in cycles beginning with an increase leading to a pulse, and ending with a period of decline. During each pulse, extensive pāhoehoe overflow units were emplaced, where-as during each phase of waning flow blockages, tubes and 'a'ā overflow units developed. Table 3 provides a summary of blockage, overflow, surge, pulse and lava tube formation events associated with each cycle, and Figs. 11 and 12 map the effects of these cycles on the channel and levee evolution. Appendices I and II provide more detailed timelines of blockage, overflow, surge, pulse and lava tube formation events during May 30 and May 31, respectively.

Pattern and frequency of flow pulses

Our data define three phases of activity (Fig. 7a and b) and five separate pulse cycles during the observation period (Table 3, Fig. 7a and b). Phase 1 was characterized by cyclic changes in the integrated temperature, which were associated with four pulse cycles during 6 h of observations (Fig. 7a). Phase 2 was a 4-h-long period during which pulses were absent and T_{int} remained roughly constant. Phase 3 was a period of pulsing activity similar to phase 1, which continued after the cessation of observations. However, T_{int} for the first pulse cycle during phase 3 (pulse cycle 5; Fig. 7b) showed a much sharper peak and shorter cycle wavelength, than in phase 1. A reversal in the thermal trend at 15:51, FLIR data and visual observation suggests that there was actually a transitory period between phases 2 and 3. Between 15:51 and 17:52 there was a small

Fig. 11 Time series of maps derived from FLIR images showing the main events in the morphological evolution of the channel during May 30. The maps are simplified versions of FLIR images and highlight the features at higher temperatures than general background temperatures. Higher temperatures are shown by lighter shades. White = hot fluid lava, black = background temperature. Stages are summarized as follows. **a** Initial channel state showing extensive, cooling pāhoehoe overflow unit (OF1) emplaced during a recent pulse. In addition a cooler (older) 'a'ā overflow unit emplaced during backup is apparent up-stream. **b** Low, post-pulse fill level leads to levees slumping and cracking. **c** Debris blockage forming at construction during increasingly sluggish flow. **d** Lateral backup related to the blockage feeds 'a'ā overflow. **e** Lateral flow stagnated; blockage still in place. **f** Blockage clearing slightly. **g** Levees growing together by accretion. **h** Levees and debris form tube. Abbreviations used are: OF = overflow, B = blockage. T = lave tube
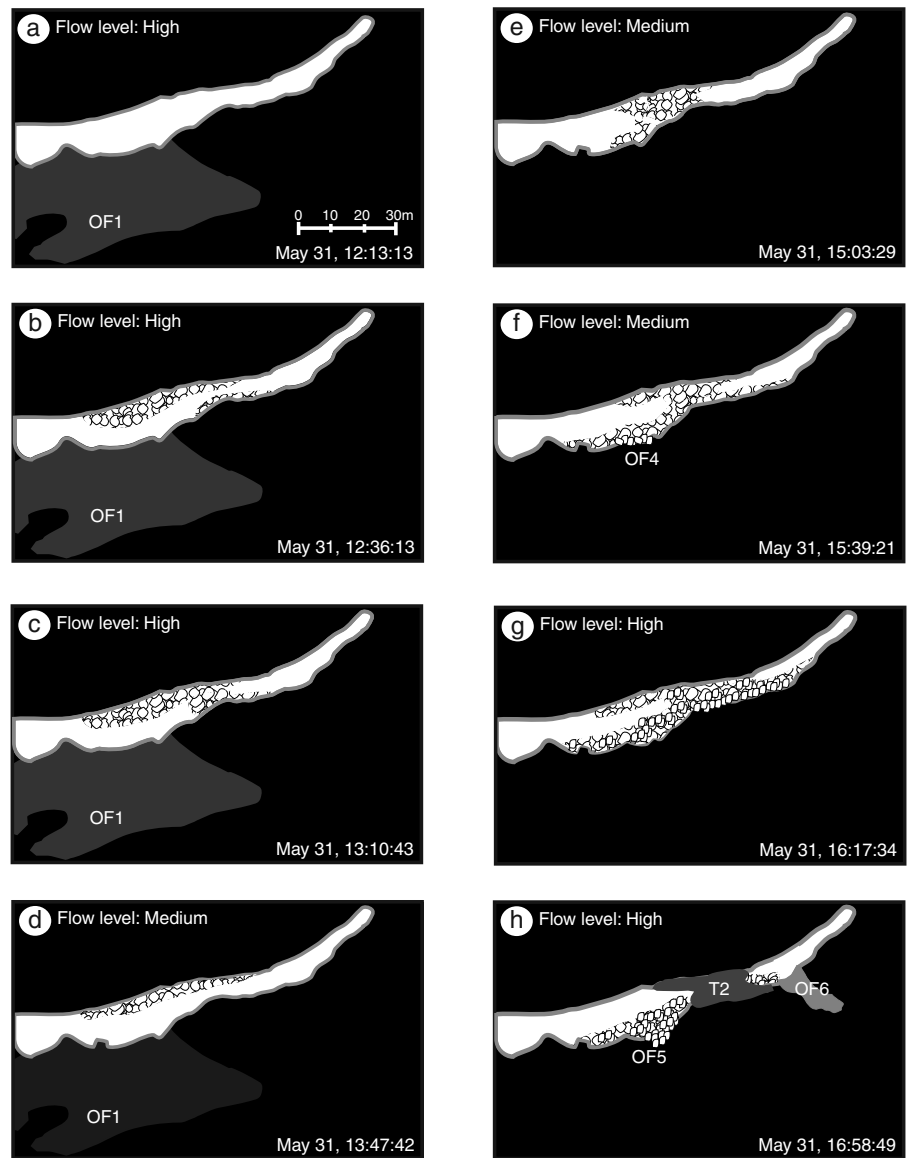
increase in channel flux and velocity that led to a few small overflows, and was followed by a waning period before the advent of pulse 5. Further observations after the conclusion of measurements suggested that wavelengths of subsequent cycles increased to values similar to those recorded the previous day.

Pattern and frequency of surge events

Surge events displayed lower thermal amplitudes but a higher frequency than pulse events. In addition, their temporal occurrence was less systematic than the cyclic behavior exhibited by the pulses. During our observations 50 surge events were identified from the FLIR data (Fig. 13). Surge events occurred, on average, once every ~9 min during May 30, and once every ~10 min on May 31. Surges were best detected using a visual analysis of the fast motion

FLIR movies to identify the down-flow propagating wave associated with each event. However, Fig. 13 gives a plot of the maximum pixel temperature encountered just down-flow of blockage site B (where most surges originated; Fig. 9) and shows that surges are always associated with a peak in the maximum temperatures, although not every peak was related to a surge. This may be explained by an increase in velocity and shearing of the flow surface during passage of the surge to expose higher temperature material. The Minolta-Land thermometer was aimed at a point upstream the blockage sites (Fig. 9), and its data do not reveal any surge-related spikes, but instead showed variations related to the pulse cycles (Fig. 13). This confirmed that the blockage was the source of the surges, and hence they are short-term increases in the discharge generated by processes that occurred within the channel itself, rather than in the conduit and/or main vent.

Fig. 12 Time series of maps derived from FLIR images showing the main events in the morphological evolution of the channel during May 31 (see Fig. 11 for explanation and key). **a** Initial channel state showing pāhoehoe overflow (OF1) still at above background temperatures. **b** Levees thickening by accretion at partial blockage. **c** Trapped debris creates full blockage. **d** Blockage partially cleared. **e** Blockage spalling and building at equal rates to maintain a constant length. **e** Blockage growing such that clinker is pushed over levee tops. **f** Lots of debris blocking channel resulting in high fill level. **g** Tube and lateral 'a'ā overflow forming

We found that surges are typically less frequent as the channel flux increases before a pulse and that surges occurred more than twice as frequently after a pulse had passed (Table 4). This was a result of the increasing velocity prior to a pulse, which allowed the channel to more efficiently carry away debris, which otherwise formed the obstructions that created surges. As flow stagnated, these blockages were more readily able to form and surges occurred more frequently. The clearing effect due to a pulse propagating along the channel only stops surges occurring for a few minutes after its passing.

Table 4 Frequency of surges during different pulse cycles

Stage in pulse cycle	Mean time between surges (min)
Pulse 2 – increase to pulse	16.32
Pulse 3 – waning period	06.80
Pulse 3 – increase to pulse	08.18
Pulse 5 – increase to pulse	15.50

Conclusions

Although the observed channel could have been described as stable in terms of its longevity and morphology, flow flux over time scales of tens of minutes to hours was far from stable. Unsteady flow, peaking at 0.7 m^3 s^{-1} and waning to 0.1 m^3 s^{-1}, typified the flow regime and a characteristic cycle could be identified (Fig. 14). Each cycle started with a high velocity (up to 0.29 m s^{-1}) pulse, which overwhelmed the channel to emplace pāhoehoe overflow units and contributed to a compound, overhanging levee form. In addition, pulses cleared any blockages and hence increased
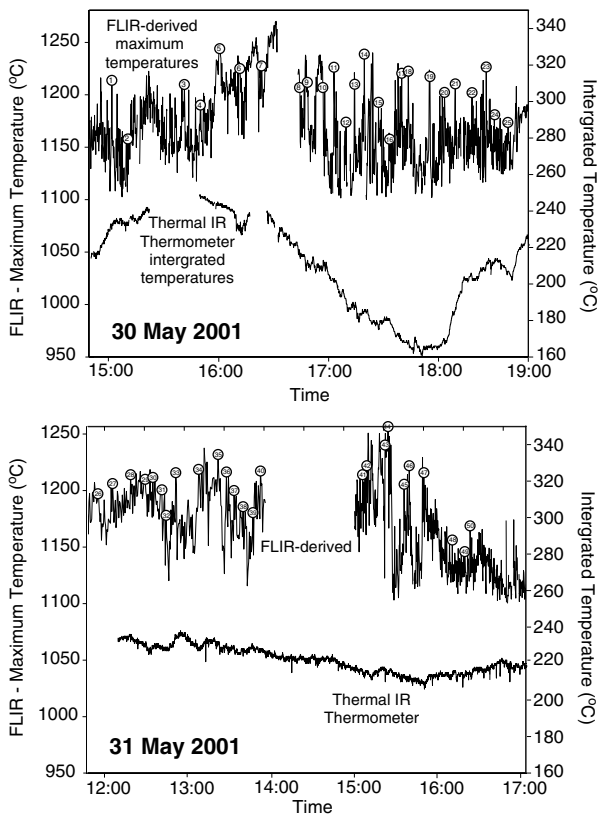
Fig. 13 Maximum FLIR-derived temperature obtained from pixels immediately downstream from blockage and thermal infrared thermometer integrated temperature trace. Surges identified from fast-motion FLIR movies are indicated with numbers
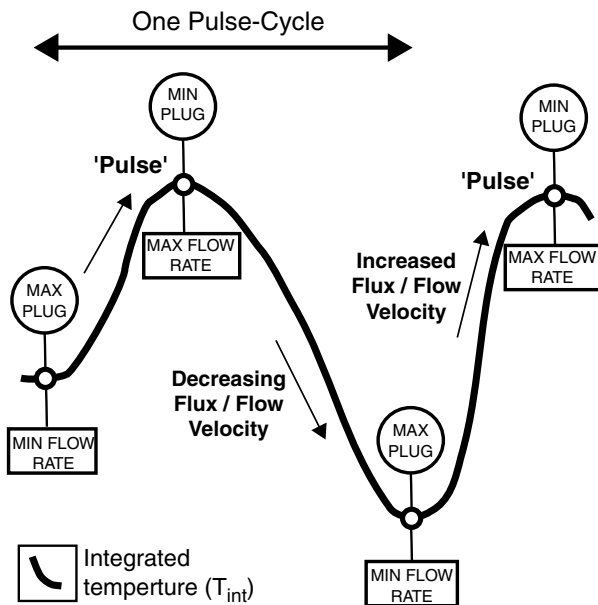

Fig. 14 Characteristics of a pulse-cycle: As the cycle builds-up to a maximum flow rate, flow velocity increases and plug width reduces to a minimum. After a pulse passes flow velocity decreases plug width increases to a maximum and flow rate reduces to a minimum. The integrated temperatures recorded by the thermal infrared thermometer show the cyclic changes

the efficiency of the channel. Pulses were followed by periods of waning flow, during which surface velocities fell to 0.05 m s^{-1}, and viscosity and yield strength increased. Blockages that formed during waning stages caused lava to backup up-stream of the blockage, and occasionally to overflow to feed slow moving 'a'ā overflows that advanced a few tens of meters down the levee flank. In the case described here, compound levees were thus symptoms of unsteady flow, where overflow levees were emplaced as relatively fast moving pāhoehoe sheets during pulses, and as slow moving 'a'ā units resulting from backup behind blockages.

We suggest that such unsteady flow may be a common feature in basaltic lava channels. Previous evidence has suggested that effusion rate changes can occur over periods of minutes to hours (Lipman and Banks 1987; Harris et al. 2000; Lautze et al. 2004). Lipman and Banks (1987), for example, observed episodic bulk volume flux variations in the 1984 Mauna Loa channel occurring over periods of minutes to hours. They noted that some of these changes reflected gas content and lava density variations rather than variations in the erupted volume flux. During the 1983 Etna eruption, fluctuations in flow velocity of ∼20% occurred over a periods of 2 to <24 h (Frazzetta and Romano 1984; Guest et al. 1987). In our case, we observe large variations in flow rate on a timescale of tens of minutes.

Our problem is that without samples we cannot tell how much of the variation in the bulk volume flux was due to variations the dense rock volume flux and how much was due to variation in the vesicularity. Our preferred hypothesis is that pulses were caused by short-term variations in the erupted flux from the vent, and involved the arrival of a batch of slightly higher temperature, lower crystallinity, and/or higher vesicularity batch with a reduced viscosity and yield strength.

Unsteady flow has implications for the collection of effusion rate data. Measurements of flow rates must consider natural, short-period variations in order to produce average values that truly reflect changes in the source effusion rate. Particular care must be taken not to use data that are falsely high due to measurement during a relatively short (and anomalous) pulse or surge period. In our case, the true eruption rate would not have been obtained unless numerous measurements were taken over a minimum 4-h period. Our results also show that scatter in effusion rate calculations may often be genuinely occurring due to unsteady flow and not due to measurement errors. New models should therefore include an adjustment that accounts for fluctuation in the effusion rate if they are considering changes in flow rheology over periods of hours or more. The FLIR thermal camera in combination with the Minolta-Land Cyclops 300 thermal infrared thermometer provide the ideal instruments to acquire the quantitative data required to make this adjustment.

512

Appendix I

Summary of events in channel on 5/30/01. The timeline provides a summary of channel activity and changes in 10-min blocks for the hours that FLIR images were captured (OF = Overflow, S = Surge, P = Surge, B = Blockage, T = Tube) Times are local time. Blockage sites refer to locations shown in Fig. 9

Time	Description of morphology changes and events
Pre-FLIR	Bifurcating flow (OF1) onto left bank near tube exit and Pahoehoe overspill (OF2) onto left bank down-flow of site B occurred due to pulse (P1) shortly before recordings began at 13:45. Small unknown-type surge (S1) just before FLIR starts recording (Fig. 11a)
14:46:27–14:56	Partial-blockage (B1) across 1/3 of channel width at site B, continuously failing and rebuilding
14:57–15:06	B1 continuing to fail and rebuild simultaneously. Medium type-1 surge (S2), a double surge as the blockage collapsed in stages
15:07–15:16	Down-flow of site B levees slumping, cracking and spalls. Blockage cleared by Medium type-1 surge (S3). Levees than begin to thickening at fill level inside channel between site B and C (Fig. 11b)
15:17–15:26	Levees continue to thickening at fill level inside channel between site B and C
15:27–15:36	Levees continue to thickening until 15:33:11 then full width blockage (B2) begins to forming across channel at site B. Blockage thickening up-flow quicker than the front spalls off
15:37–15:46	B2 still building. Some small type-1 surges (S4, S5) related to front of blockage spall (Fig. 11c)
15:47–15:56	B2 still building
15:57–15:56	B2 still building. Small type-1 surge (S6)
15:57–16:06	Break in FLIR coverage
16:07–16:16	Lateral 'a'a flow (OF3) becomes active up-flow of site C down left bank, at 16:08:01. B2 still building at back but is pushed forward to replace front that spalls off at same rate. Medium type-2O surge (S7)
16:17–16:26	OF3 and B2 continuing as before. Double small type-1surge (S8) (Fig. 11d)
16:27–16:28	OF3 and B2 continuing as before
16:29–16:38	Break in FLIR coverage
16:39–16:48	OF3 continuing. B2 also continuing as before but losing more material than it is adding, so overall length is shortening. Small type-1 surge (S9) seen mostly as a spurt forward of OF3. Small type-2U surge (S10) drains under blockage and rips away part of its front without releasing any obvious secondary surge. OF3 is a consequence of pulse (P2) weakening levees
16:49–16:58	Small type-1 surge (S11). OF3 stops actively flowing at 16:58:24. Large type-1 surge (S12) occurs after OF3 no longer being fed. B2 continues to lose length (Fig. 11e)
16:59–17:08	B2 continues to lose length. Small type-1 surge (S13)
17:09–17:18	B2 continues to lose length until 17:13:54 when blockage breaking apart. Small type-1 (S14) and then large type-1 (S15) surges
17:19–17:28	B2 now only partial. As front breaks apart large double surge (S16) generated, initially of type-1 and then type-2O. Medium type-1 then type-2O surge (S17) (Fig. 11f)
17:29–17:38	B2 is an increasingly smaller partial-blockage; unstable. Double surge (S18) mostly of type-2O nature. Small type-2U surge (S19)
17:39–17:48	B2 is an increasingly smaller partial-blockage; unstable
17:49–17:58	B2 all cleared by 17:57:44. Levees thickening at fill level around site B. Medium triple Surge (S20) made up of two type-1 and one type-2O. Medium type-2O surge (S21) (Fig. 11g)
17:59–18:08	Levees continue to thicken. Small type-2O surge (S22) helps clear loose debris by levees near site B
18:09–18:18	Levees continue to thicken. Small type-2O surge (S23) over thickened levee bases. Down-flow of site B levees slumping as surge clear out channel debris and fill level lowers
18:19–18:28	Levees thickening at fill level around site B. Medium type-2U surge (S24) over thickened levees. By 18:20:04 levees connected to form thin crust across channel. Crust thickens and starts to form solid tube (T1). Medium type-2O surge (S25) tries to flow over the top of the tube during infancy of formation
18:29–18:38	Little spall off front of solid tube. Small type-2U surge (S26) flows through tube without causing destruction (Fig. 11h)
18:39–18:43:05	Tube still intact
Post-FLIR	Tube still intact until overwhelmed and destroyed by pulse (P3) at ~19:30. Another pulse-cycle (P4) starts at 20:23

Appendix II

Summary of events in channel on 5/31/01 using the same
format and nomenclature used in Appendix I

Time	Description of morphology changes and events
Pre-FLIR	Partial blockage (B4) continually forming and being destroyed at site B. Very uneven flow. B4 still continually forming and being destroyed. Small Type-1 surge (S27)
11:49–12:08	B4 still continually forming and being destroyed. Small Type-1 surge (S28)
12:09–12:18	B4 still continually forming and being destroyed (Fig. 12a)
12:19–12:28	B4 still continually forming and being destroyed. Small type-2U surge (S29) forced under thick levees
12:29–12:38	B4 still continually forming and being destroyed. Small type-2U surge (S30) forced under. Medium type-2O surge (S31) tries to flow over blockage which causes it to collapse turning S31 into a type-1 event (Fig. 12b)
12:39–12:48	Medium type-1 (S32) and small type-2O (S33) surges clear blockage from center of channel but remnants at base of levees enable P4 to form again
12:49–12:58	Medium type-2U double surge (S34) at 12:51:43 clears the debris forming B4 from site B, but levees in this section start to thicken and spread across the channel
12:59–13:08	Thickened levee at site B connects into full width blockage (B5) at 13:05:13. Small type-2U surge (S35)
13:09–13:18	B5 intact (Fig. 12c)
13:19–13:28	B5 intact until 13:23:13 then starts breaking up and becomes a partial blockage. Large type-1 (S36) and medium type-1 (S37) surges
13:29–13:38	B5 being steadily cleared but a thick crust remains intact at the base of the levees near site B. Large type-1 double surge (S38)
13:39–13:48	B5 being steadily cleared. Medium type-2U (P39) and small type-2O (S40) surges (Fig. 12d)
13:49–13:57	Channel mostly cleared, but bases of levees at site B still thick. Small type-2O double surge (S41)
13:58–15:02	Break in FLIR coverage
15:02–15:11	Solid blockage (B6) at site B spalls at front but building at back at same rate, and then shifts down-flow slightly to maintain blockage at same location. Small type-1 (S42) and medium type-1 (S43) surges (Fig. 12e)
15:12–15:21	B6 maintaining balance between construction and destruction, and continues to shift new debris down-flow to maintain overall position
15:22–15:31	B6 balance maintained until 15:26:06 when it is broken into a partial blockage. Two medium type-1 surges (S44, S45) generated. Clinker levees being pushed up at and down-flow from site B
15:32–15:41	B6 remains as partial blockage, clinker levees continue to be pushed up. Small type-1 (S46) and Medium type-1 (S47) surges lead to small overspill (OF4) onto levees between sites B and C (Fig. 12f)
15:42–15:51	B6 remains until 15:46:05 when large type-2O surge (S48) clears out the blockage at site B. Almost immediately viscous crust stagnates and reforms a blockage (B7) at site C
15:52–16:01	B7 remains intact. Levees at site A thicken and grow across channel; Lava backing-up at different levels behind both blockages
16:02–16:11	B7 at site C and growing levees at site A. Lava flow restricted at different levels
16:12–16:21	Lava flow still restricted at two levels. Blockage at site A (B8) fully formed by 16:17:04. Small type-2U (S49) and type-1 (S50) surges then clear B7 (Fig. 12g)
16:22–16:31	B8 becoming more solid. Down-flow of site B parts of inner levees collapse and are overwhelmed by lava. Medium type-1 surge (S51)
16:32–16:41	B8 more solid and forming a tube (T2). Small overspill (OF5) onto levee tops down-flow of site B
16:42–16:51	B8 building as a tube. At 16:51:34 lava is diverted down left bank as a lateral 'a'a flow (OF6). Increased flow rate a result of pulse (P5)
16:52–17:01	B8 building as a tube. OF6 still active (Fig. 12h)
17:02–17:05:04	B8 building as a tube. OF6 still active
Post-FLIR	OF6 stops at 17:33. Tube and debris cleared out of channel by pulse (P6) ∼18:45, which produces channel overspills (OF7) and a forms a bifurcating flow down right bank. Flow still developing into a permanent channel branch at end of observations

References

Andronico D, Branca S, Calvari S, Burton MR, Caltabiano T, Corsaro RA, Del Carlo P, Garfì G, Lodato L, Miraglia L, Muré F, Neri M, Pecora E, Pompilio M, Salerno G, Spampinato L (2005) A multi-disciplinary study of the 2002–03 Etna eruption: insights for into a complex plumbing system. Bull Volcanol 64:314–330, doi:10.1007/s00445-004-0372-8

Baloga S, Pieri D (1986) Time-dependent profiles of lava flows. J Geophys Res 91:9543–9552

Behncke B, Neri M (2003) The July-August 2001 eruption of Mt. Etna (Sicily). Bull Volcanol 65:461–476

Bonaccorso A, Calvari S, Garfì G, Lodato L, Patané D (2003) December 2002 flank failure and tsunami at Stromboli volcano inferred by volcanological and geophysical observations. Geophys Res Lett 30:1941–1944

Calvari S and research staff of the Instituto Nazionale di Geofisica e Vulcanologia – Sezione di Catania, Italy (2001) Multidisciplinary approach yields insight into Mt. Etna eruption. Eos Trans AGU 82(52): 653, 656

Calvari S, Pinkerton H (1998) Formation of lava tubes and extensive flow field during the 1991–93 eruption of Mount Etna. J Geophys Res 103:27291–27302

Calvari S, Pinkerton H (1999) Lava tube morphology on Etna and evidence for lava flow emplacement mechanisms. J Volcanol Geotherm Res 90:263–280

Calvari S, Neri M, Pinkerton H (2002) Effusion rate estimations during the 1999 summit eruption on Mount Etna, and growth of two distinct lava flow fields. J Volcanol Geotherm Res 119:107–123

Calvari S, Coltelli M, Neri M, Pompilio M, Scribano V (1994) The 1991–93 Etna eruption: chronology and geological observations. Acta Vulcanol 4:1–15

Cashman KV, Thornber C, Kauahikaua J (1999) Cooling and crystallization of lava in open channels, and the transition of pāhoehoe lava to ʻaʻā. Bull Volcanol 61:306–323

Cigolini C, Borgia A, Castertano L (1984) Intracrater activity, ʻaʻā-block lava, viscosity and flow dynamics: Arenal volcano, Costa Rica. J Volcanol Geotherm Res 20:155–176

Crisp J, Baloga S (1990) A model for lava flows with two thermal components. J Geophys Res 95:1255–1270

Crisp J, Baloga S (1994) Influence of crystallization and entrainment of cooler material on the emplacement of basaltic ʻaʻā lava flows. J Geophys Res 99:11819–11831

Crisp J, Cashman KV, Bonini JA, Hougen SB, Pieri D (1994) Crystallization history of the 1984 Mauna Loa lava flow. J Geophys Res 95:7177–7198

Dehn J, Dean KG, Engle K, Izbekov P (2002) Thermal precursors in satellite imagery of the 1999 eruption of Shishaldin. Bull Volcanol 64:525–534

Dehn J, Harris AJL, Ripepe M (2001) Conduit convection insights from thermal measurements of gas puffing at Stromboli and Etna. Eos Trans AGU 82(47), Fall Meet Suppl, Abstract V52C-01

Dehn J, Harris AJ, Patrick MR, Calvari S, Lodato L, Ripepe M (2003) Lava extrusion rates from handheld infrared imagery. *Eos Trans AGU 84*(46), Fall Meet Suppl, Abstract V51F-0333

Dragoni MA (1989) A dynamical model of lava flows cooling by radiation. Bull Volcanol 51:88–95

Dragoni M, Tallarico A (1994) The effect of crystallization on the rheology and dynamics of lava flows. J Volcanol Geotherm Res 59:241–252

Dragoni M, Bonafede M, Boschi E (1986) Downslope flow models of a Bingham liquid: implications for lava flows. J Volcanol Geotherm Res 30:05–325

Dragoni M, Pondrelli S, Tallarico A (1992) Longitudinal deformation of a lava flow: the influence of Bingham rheology. J Volcanol Geotherm Res 52:247–254

Flynn LP, Mouginis-Mark P (1994) Temperature of an active lava channel from spectral measurements, Kilauea Volcano, Hawaii. Bull Volcanol 56:297–301

Frazzetta G, Romano R (1984) The 1983 Etna eruption: event chronology and morphological evolution of the lava flow. Bull Volcanol 47:1079–1096

Griffiths RC, Kerr RC, Cashman KV (2003) Patterns of solidification in channel flows with surface cooling. J Fluid Mech 496:33–62

Guest JE, Kilburn CRJ, Pinkerton H, Duncan AM (1987) The evolution of lava flow-fields: observations of the 1981 and 1983 eruptions of Mount Etna, Sicily. Bull Volcanol 49:527–540

Harris AJL, Rowland SK (2001) FLOWGO: a kinematic thermo-rheological model for lava flowing in a channel. Bull Volcanol 63:20–44

Harris AJL, Flynn LP, Matías O, Rose WI (2002) The thermal stealth flows of Santiaguito: implications for the cooling and emplacement of dacitic block lava flows. Geol Soc Am Bull 114:533–546

Harris AJL, Blake S, Rothery DA, Stevens NF (1997) A chronology of the 1991 to 1993 Mount Etna eruption using advanced very high resolution radiometer data: implications for real-time thermal volcano monitoring. J Geophys Res 102:785–803

Harris AJL, Dehn J, Patrick M, Calvari S, Ripepe M, Lodato L (1995) Lava effusion rates from handheld thermal infrared imagery: an example from the June 2003 effusive activity at Stromboli. Bull Volcanol 68:107–117. doi:10.1007/s00445-005-0425-7

Harris AJL, Flynn LP, Keszthelyi L, Mouginis-Mark PJ, Rowland SK, Resing JA (1998) Calculation of lava effusion rates from Landsat TM data. Bull Volcanol 60:52–71

Harris AJL, Murray JB, Aries SE, Davies MA, Flynn LP, Wooster MJ, Wright R, Rothery DA (2000) Effusion rate trends at Etna and Krafla and their implications for eruptive mechanisms. J Volcanol Geotherm Res 102:237–270

Hulme G (1974) Interpretation of lava flow morphology. Royal Astron Soc Geophys J 39:361–383

Ishihara K, Iguchi M, Kamo K (1990) Numerical simulation of lava flows on some volcanoes in Japan. In: Fink JH (ed) Lava flows and domes, Springer, Berlin Heidelberg New York, pp 184–207

Kerr RC (2001) Thermal erosion by laminar lava flows. J Geophys Res 106:26453–26465

Keszthelyi L (1995) Measurements of cooling at the base of pāhoehoe flows. Geophys Res Lett 22:2195–2198

Keszthelyi L, Self S (1998) Some physical requirements for the emplacement of long basaltic lava flows. J Volcanol Geotherm Res 103:27447–27464

Keszthelyi L, Harris AJL, Dehn J (2003) Observations of the effect of wind on the cooling of active lava flows. Geophys Res Lett 30:1989–1992

Kilburn CRJ (1990) Surfaces of ʻaʻā flow-fields on Mount Etna, Sicily: morphology, rheology, crystallization and scaling phenomena. In: Fink JH (ed) IAVCEI Proceedings in Volcanology, 2, Lava flows and domes: emplacement mechanisms and hazard implications, Springer, Berlin Heidelberg New York, pp 129–156

Kilburn CRJ (2000) Lava flows and flow fields. In: Sigurdsson H (ed), Encyclopedia of volcanoes, Academic, San Diego, pp 291–306

Kilburn CRJ, Guest JE (1993) ʻaʻā lavas of Mount Etna, Sicily. In: Kilburn CRJ, Luongo G (eds) Active Lavas: monitoring and modeling, Univ. College of London Press, pp 73–106

Kilburn CRJ, Lopes RMC (1988) The growth of ʻaʻā flow-fields on Mount Etna, Sicily. J Geophys Res 93:14759–14772

Lautze NC, Harris AJL, Bailey JE, Ripepe M, Calvari S, Dehn J, Rowland S (2004) Pulsed lava effusion at Mount Etna during 2001. J Volcanol Geotherm Res 137:231–246

Lipman PW, Banks NG (1987) ʻaʻā flow dynamics, Mauna Loa 1984. In: Decker RW, Wright TL, Stauffer PH (eds) Volcanism in Hawaii, vol 1350. US Geol Surv Prof Pap, pp 1527–1567

Macdonald GA (1953) pāhoehoe, ʻaʻā and block lava. Am J Sci 251:169–191

McGimsey RG, Schneider DJ, Neal CA, Roach AL (1999) Use of FLIR observations during eruption response at two Alaskan volcanoes. *Eos Trans AGU 80(46),* Fall Meet Suppl, Abstract V32A-07

Moore HJ (1987) Preliminary estimates of the rheological properties of 1984 Mauna Loa lava. US Geol Surv Prof Pap 1350:1569–1588

Naranjo JA, Sparks RSJ, Stasiuk MV, Moreno H, Ablay GJ (1992) Morphological, structural and textural variations in the 1988–1990 andesite lava of Lonqimay volcano, Chile. Geol Mag 129:657–678

Oppenheimer C, Yirgu G (2002) Thermal imaging of an active lava lake; Erta 'Ale Volcano, Ethiopia. Int J Remote Sens 23:4777–4782

Patrick MR, Harris A, Dehn J, Ripepe M, Calvari S (2003) FLIR thermography and heat/mass budgets bound the 2002/2003 effusive period at Stromboli volcano. Eos Trans AGU 84(46), Fall Meet Suppl, Abstract V52C-02

Peterson DW, Holcomb RT, Tilling RI, Christiansen RL (1994) development of lava tubes in the light of observations at Mauna Ulu, Kilauea Volcano, Hawaii. Bull Volcanol 56:343–360

Pieri DC, Glaze LS, Abrams MJ (1990) Thermal radiance observations of an active lava flow during the June 1984 eruption of Mount Etna. Geology 18:1018–1022

Pinkerton H, Sparks RSJ (1976) The 1975 subterminal lavas, Mount Etna: a case history of the formation of a compound lava field. J Volcanol Geotherm Res 1:167–182

Pinkerton H, Wilson L (1994) Factors controlling the lengths of channel-fed lava flows. Bull Volcanol 56:108–120

Polacci M, Papale P (1997) The evolution of lava flows from ephemeral vents at Mount Etna: insights from vesicle distribution and morphological studies. J Volcanol Geotherm Res 76:1–17

Rossi MJ (1997) Morphology of the 1984 open-channel lava flow at Krafla volcano, northern Iceland. Geomorphology 20:95–112

Rowland SK, Walker GPL (1990) Pāhoehoe and 'a'ā in Hawai'i: volumetric flow rate controls the lava structure. Bull Volcanol 52:615–628

Sparks RSJ, Pinkerton H, Hulme G (1976) Classification and formation of lava levees on Mount Etna, Sicily. Geology 4:269–271

Tallarico A, Dragoni M (1999) Viscous Newtonian laminar flow in a rectangular channel: application to Etna lava flows. Bull Volcanol 61:40–47

Wadge G (1981) The variation of magma discharge during basaltic eruptions. J Volcanol Geotherm Res 11:139–168

Walker GPL (1967) Thickness and viscosity of Etnean lavas. Nature 213:484–485

Walker GPL (1972) Compound and simple lava fields and flood basalts. Bull Volcanol 35:579–590

Wright R, Flynn LP (2003) On the retrieval of lava flow surface temperatures from infrared satellite data. Geology 31:893–896

Wright R, Flynn LP, Harris AJL (2001) The evolution of lava flow fields at Mount Etna, 27–28 October 1999, observed by Landsat 7 ETM+. Bull Volcanol 63:1–7

Wright R, Rothery DA, Blake S, Pieri DC (2000) Visualising active volcanism with high spatial resolution satellite data: the 1991–1993 eruption of Mount Etna. Bull Volcanol 62:256–265